C. R. Mecanique 340 (2012) 139–155

Contents lists available at SciVerse ScienceDirect

Comptes Rendus Mecanique

www.sciencedirect.com

Multi-objective optimization to predict muscle tensions in a pinch function using genetic algorithm

Amani Bensghaier [a,*], Lotfi Romdhane [b], Fethi Benouezdou [c]

[a] Laboratoire de génie mécanique LGM, École nationale d'ingénieurs de Monastir LGM-ENIM, Monastir, Tunisia
[b] Laboratoire de génie mécanique LGM, École nationale d'ingénieurs de Sousse ENISO, Sousse, Tunisia
[c] Laboratoire d'ingénierie des systèmes LISV, Université de Versailles Saint Quentin, site de Vélizy, 10-12, avenue de l'Europe, 78140 Vélizy, France

ARTICLE INFO

Article history:
Received 15 January 2010
Accepted after revision 6 January 2012
Available online 8 February 2012

Keywords:
Biomechanics
Tip pinch
Muscle tensions prediction
Multi-objective optimization
Genetic algorithm
Index finger
Thumb

ABSTRACT

This work is focused on the determination of the thumb and the index finger muscle tensions in a tip pinch task. A biomechanical model of the musculoskeletal system of the thumb and the index finger is developed. Due to the assumptions made in carrying out the biomechanical model, the formulated force analysis problem is indeterminate leading to an infinite number of solutions. Thus, constrained single and multi-objective optimization methodologies are used in order to explore the muscular redundancy and to predict optimal muscle tension distributions. Various models are investigated using the optimization process. The basic criteria to minimize are the sum of the muscle stresses, the sum of individual muscle tensions and the maximum muscle stress. The multi-objective optimization is solved using a Pareto genetic algorithm to obtain non-dominated solutions, defined as the set of optimal distributions of muscle tensions. The results show the advantage of the multi-objective formulation over the single objective one. The obtained solutions are compared to those available in the literature demonstrating the effectiveness of our approach in the analysis of the fingers musculoskeletal systems when predicting muscle tensions.

© 2012 Académie des sciences. Published by Elsevier Masson SAS. All rights reserved.

1. Introduction

It has always been desirable to explore the mechanics of the fingers and the tendons as an aid in clinical treatment such as tendon transfers, prevention protocols, and rehabilitation efficacy [1]. Unfortunately, there is no device to directly measure muscle tensions [2]. As a consequence, biomechanical models of the hand become a necessary tool to analyze different aspects of the musculoskeletal systems [3–6]. However, the thumb and the index finger systems, considered in this work, are highly redundant, i.e., the number of independent muscles acting on a particular joint exceeds the number of degrees of freedom of that joint. Hence, there is no direct or unique pattern in terms of the required muscle forces when performing a specific pinch task. Several models, which are based on optimization techniques, have been proposed over the last few decades to solve this indeterminate problem [7–11]. However most of the anatomical and biomechanical analyses of hand functions, that have been conducted to provide predictions of muscle tensions, are often based on mono-criterion optimization process.

On the other hand, numerical optimization techniques based on heuristic methods and the Pareto optimality concept have been often used in the fields of biomechanics, engineering and science [12–14]. Multi-objective optimization based on

* Corresponding author.
E-mail addresses: amani.bsghaier@gmail.com (A. Bensghaier), lotfi.romdhane@enim.rnu.tn (L. Romdhane), ouezdou@lisv.uvsq.fr (F. Benouezdou).

1631-0721/$ – see front matter © 2012 Académie des sciences. Published by Elsevier Masson SAS. All rights reserved.
doi:10.1016/j.crme.2012.01.002

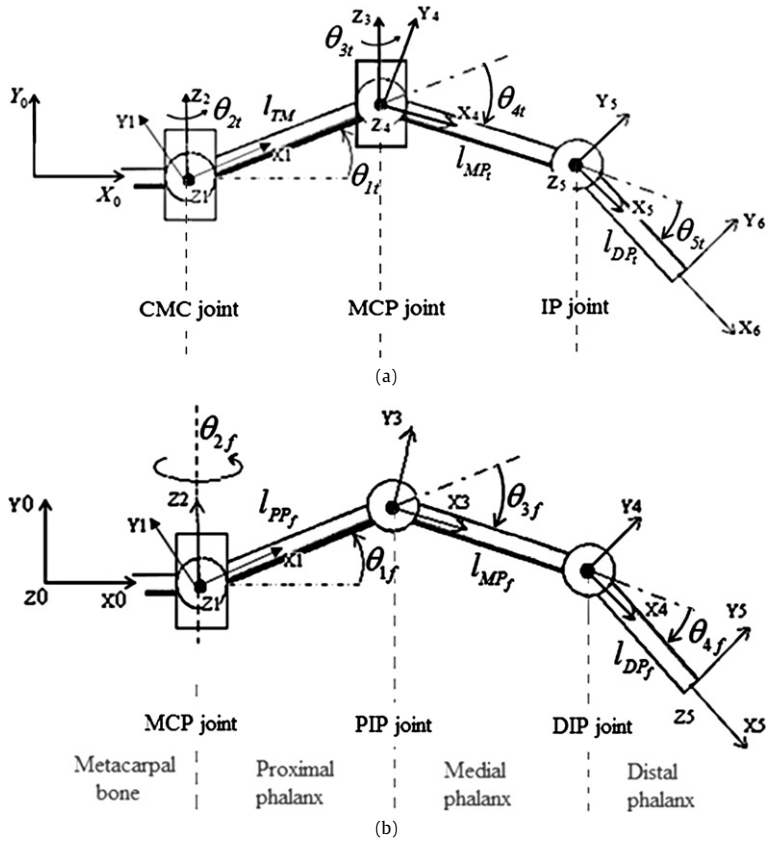

Fig. 1. (a) Kinematic model of the thumb. $l_{TM} = 5.29$ cm, $l_{MP_t} = 4.5$ cm and $l_{DP_t} = 3.2$ cm are the lengths of the trapezio-metacarpal, the middle and the distal thumb segments. (b) Kinematic model of the index finger. $l_{PP_f} = 5$ cm, $l_{MP_f} = 3.1$ cm and $l_{DP_f} = 1.6$ cm are the lengths of the proximal, the middle and the distal index finger segments, respectively.

genetic algorithm is also used in several works [15–17]. Nevertheless, this technique has never been used to predict muscle tensions in the human hand musculoskeletal system.

The goal of the current study is to develop and solve a biomechanical model of the thumb and the index finger using multi-objective evolutionary optimization technique. A static analysis of the musculoskeletal thumb and index finger is performed. To establish the studied apparatus model, equivalent mechanical multi-limbs and multi-joint systems are chosen. The relative joints orientations in a tip pinch position are determined. Kinematic models with five DOF and four DOF are assumed for the thumb and the index finger, respectively. Single and multi-objective optimization processes, based on genetic algorithms, are implemented to obtain optimal muscle tensions in a static fingers posture. The predictions of different computed models are compared. Simulation results are presented and discussed showing the effectiveness of using single and multi-objective Pareto front based resolution.

2. Thumb and index finger: Biomechanical models

It is of a great importance to understand the functional mechanism related to the musculoskeletal system. In a general pollici-digital pinch, only the thumb and the index finger are active. Since our study is focusing on tip pinch task, an anatomical study is performed to describe the characteristics of each finger multi-DOF joints. Then a representative mechanical model is built for each finger. We neglect in the developed model the carp-bones relative motion. Thanks to biomaterial tissues, the chosen joints are also assumed to be frictionless.

2.1. Anatomy and kinematics of the thumb

The thumb is assumed to have five degrees of freedom (DOF) [2] linking three successive phalanxes to the metacarpal bone. The carpo–metacarpo phalangeal (CMC) and the metacarpo-phalangeal (MCP) joints are approximated with universal joints (two DOF). Each universal joint reproduces the flexion–extension and the adduction–abduction movements. The interphalangeal (IP) joint is modelled as a hinge joint, which is able to perform only the flexion–extension movement.

Different notations required to establish the thumb kinematic model and to express its structure are given in Fig. 1(a). The axes X_0, Y_0 and Z_0 are attached to the metacarpal bones and represent the global reference frame. The joint rotational

Table 1
Components included in the biomechanical model.

Finger	Muscle	Abbreviation	PCSA (cm^2)
Thumb	Flexor pollicis longus	FPL	3.5
	Extensor pollicis longus	EPL	1.9
	Flexor pollicis brevis	FPB	1.2
	Extensor pollicis brevis	EPB	1.3
	Abductor pollicis brevis	APB	1.5
	Adductor pollicis	ADD	0.8
	Opponens pollicis	OP	2.8
	Abductor pollicis longus	APL	3.9
Index finger	Flexor digitorium profundus	FDP	4.1
	Flexor digitorium superficialis	FDS	4.2
	Extensor digitorium communis	EDC	1.39
	Extensor indicis	EI	1.12
	Radial interosseous	RI	4.16
	Ulnar interosseous	UI	1.6
	Lumbrical	LUM	0.36

Note: $PCSA_i$ is the physiological cross-sectional area of the ith muscle.

axes (Z_1, Z_2) coincide with the rotational axes of the CMC joint. Vectors Z_3 and Z_4 represent the rotational axes of the MCP joint while Z_5 designates the rotational axis of the IP joint. The axes X_6, Y_6 and Z_6 define the frame fixed to the index fingertip.

The thumb has eight muscles which are described in Table 1. All muscles are represented in Fig. 2(a). The FPB and the OP muscles control the flexion movement of the CMC joint. The EPL and the EPB muscles actuate the extension movement. The APL and the APB muscles generate the abduction movement whereas the ADD muscle produces the adduction movement. Finally, the OP muscle controls the combined opposition movement. For the MCP joint, the flexion movement is actuated by the FPL and the FPB muscles while the extension is generated by the EPL and the EPB muscles. For the IP joint, only one flexor, the FPL and one extensor, the EPL cross this joint and insert into the thumb distal phalanx.

2.2. Anatomy and kinematics of the index finger

The index finger is assumed to have only four DOF [18]. A universal joint models the flexion–extension and the adduction–abduction movements of the MCP joint. Two hinge joints (one DOF) are used to model the flexion–extension of the proximal interphalangeal (PIP) and the distal interphalangeal (DIP) joints.

The different coordinate systems and segment lengths used to compute the kinematic model of the index finger are described in Fig. 1(b). The joint axes (Z_1, Z_2) match with the rotational axes of the MCP joint, which are the flexion–extension and the abduction–adduction axes respectively. Vectors Z_3 and Z_4 represent the flexion/extension axes of the PIP and the DIP joints, respectively. The axes X_5, Y_5 and Z_5 define the frame fixed to the index fingertip.

The index finger has seven extrinsic muscles, which are described in Table 1. These muscles are responsible of the movements of the index finger phalanges. For the first phalanx, the RI, the UI and the LUM muscles, assisted by the FDP and the FDS muscles, actuate the flexion movement. The extension movement of the first phalanx is controlled by both the EDC and the EI muscles, whereas, the abduction movement is actuated by the RI muscle and the adduction one by the UI muscle. The FDS muscle actuates the flexion of the second phalanx, while the FDP muscle generates flexion movement of the third phalanx. The extension of the interphalangeal index joints (DIP and PIP) is controlled by the complex extension apparatus (Fig. 2(b)), which is made of a tendinous extensor network that wraps over the dorsum of the finger phalanx. This extension apparatus is composed of the terminal extensor (TE), the extensor slip (ES), the radial band (RB) and the ulnar band (UB).

The force transmitted to the extensor mechanism cannot be determined experimentally nor by geometrical computation, except the fraction of the force transmitted by the radial band and the ulnar one to the terminal extensor (TE) [3]. This model can be written as:

$$F_{TE} = \chi_{RB} F_{RB} + \chi_{UB} F_{UB} \tag{1}$$

The coefficients χ_{RB} and χ_{UB} are the cosine terms accounting for the convergence angles of the RB and UB tendons on the TE one. The numerical values of these coefficients are $\chi_{RB} = 0.992$ and $\chi_{UB} = 0.995$ [3]. The same coefficients are later used by Brook et al. [10] and Vigouroux [11]. The remaining proportions of the transmitted force to the extensor mechanism are varying according to the relative flexion angles of the MCP and the PIP joints [19]. Vigouroux [11] proposed to represent these proportions by α_k unknown coefficients (2).

$$\begin{aligned} F_{RB} &= \alpha_{EDC} F_{EDC} + \alpha_{LUM} F_{LUM} \\ F_{UB} &= \alpha_{EDC} F_{EDC} + \alpha_{UI} F_{UI} \\ F_{ES} &= (1 - \alpha_{UI}) F_{UI} + (1 - \alpha_{LUM}) F_{LUM} + (1 - 2\alpha_{EDC}) F_{EDC} \end{aligned} \tag{2}$$

where F_i defines the tension of the ith muscle.

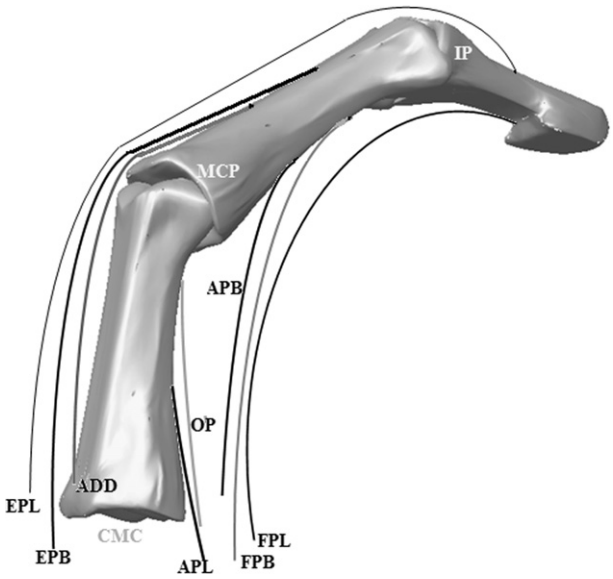

(a)

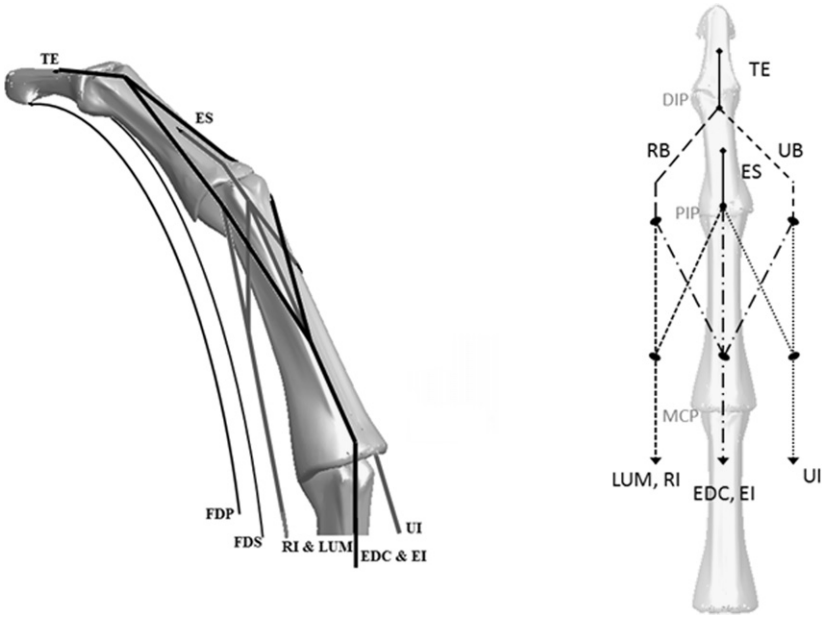

(b)

Fig. 2. (a) Thumb muscles paths. (b) Index finger muscles paths and schematic representation of tendon junctions in the extensor mechanism.

These coefficients will be included in the unknown vector and will be determined with the unknown muscle tensions using the optimization process. Finally, for the considered thumb and index finger system, the total number of considered muscles is fifteen whereas the number of degrees of freedom is nine. Therefore, the musculoskeletal system, made of the two fingers, is redundantly actuated.

2.3. The fingertip loadings and the corresponding joint torques

The reference frame, fixed to the thumb-tip axes X_6, Y_6 and Z_6 define the distal, the dorsal and the lateral force directions, respectively (Fig. 1(a)). The axes X_5, Y_5 and Z_5, shown in Fig. 1(b), are the axes of the reference frame fixed to the index fingertip. They also define the distal, the dorsal and the lateral force directions, respectively. The wrench applied on each fingertip can be written as a six-dimensional vector of fingertip forces and moments (3).

$$\boldsymbol{F}_{ext_n} = [\, f_{x_n} \quad f_{y_n} \quad f_{z_n} \quad \tau_{x_n} \quad \tau_{y_n} \quad \tau_{z_n} \,]^T \tag{3}$$

where $n =$ the thumb or the index finger.

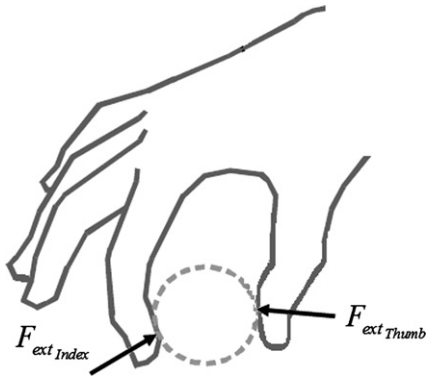

Fig. 3. Posture adopted by the thumb and the index finger to insure a tip pinch task. The coordinates of the contact point on the index finger distal phalanx p_x, p_y and p_y are equal respectively to 1 cm, −0.5 cm and 0. The considered contact point coordinates on the thumb distal phalanx are $p_x = 2$ cm, $p_y = 0$ and $p_z = 0$.

Table 2
Joint orientation angles for a tip pinch.

Finger	Degree of freedom	Notation	Angle (degree)
Thumb	CMC extension	θ_{1t}	24
	CMC adduction	θ_{2t}	−25
	MCP adduction	θ_{3t}	−5
	MCP extension	θ_{4t}	−25
	IP extension	θ_{5t}	−10
Index finger	MCP extension	θ_{1f}	−48
	MCP adduction	θ_{2f}	0
	PIP extension	θ_{3f}	−50
	DIP extension	θ_{4f}	−25

In this work, only the tip pinch study is considered (Fig. 3). The index finger and the thumb are assumed to act on the object through contact points. Since a very low friction between the fingertips and the object is assumed, the contact can be considered frictionless.

The single contact point model leads to the fact that no fingertip torques will be produced (4). Moreover, the entire fingertip force will be exerted only along the normal direction (the dorsal direction in the developed model). The distal and the lateral fingertip force components have to be equal to zero, Eq. (4).

$$\tau_{x_n} = \tau_{y_n} = \tau_{z_n} = 0, \qquad f_{x_n} = f_{z_n} = 0 \tag{4}$$

where $n =$ the thumb or the index finger.

For the index finger (respectively for the thumb), the vector of fingertip forces and torques represented at the contact point in the (X_5, Y_5, Z_5) (respectively (X_6, Y_6, Z_6)) coordinate frame is given by Eq. (5) (respectively (6)) as follows:

$$\boldsymbol{F}_{ext_{Index}} = [\,0 \quad 10 \quad 0 \quad 0 \quad 0 \quad 0\,]^T \tag{5}$$

$$\boldsymbol{F}_{ext_{Thumb}} = [\,0 \quad 10 \quad 0 \quad 0 \quad 0 \quad 0\,]^T \tag{6}$$

As only static analysis is considered in this paper, Table 2 gives the measured values of the thumb and of the index finger joint angles defining the tip pinch configuration. The static equilibrium of the tip pinch configuration needs a set of joint torques, which can be established using the virtual work principle since all joints are assumed to be frictionless. The joint torques vector $\boldsymbol{M}_{Fext_n}$ can be established using the Jacobian transpose matrix (7). It is well known that Jacobian matrix depends on the phalanx lengths and joint angles (see Appendix A).

$$\boldsymbol{M}_{Fext_n} = \mathbf{J}_n^T \boldsymbol{F}_{ext_n}, \quad n = \text{the thumb or the index finger} \tag{7}$$

where:

- $\boldsymbol{F}_{ext_n}$ is the forces and torques vector applied on the fingertip reference frame.
- $\mathbf{J}_n^T$ defines the Jacobian transpose matrix, which is four by six for the index finger and five by six for the thumb.
- $\boldsymbol{M}_{Fext_n} = (M_{Fext_j})$ defines the joint torque vector (Table 3) resulting from the application of the fingertip forces and torques. Each torque M_{Fext_j} is written in the corresponding joint reference frame. $j = CMC_f, CMC_a, MCP_a, MCP_f$, and IP if $n =$ the thumb and $j = MCP_f, MCP_a, PIP$ and DIP if $n =$ the index finger.

Table 3
Joint torques induced by the external loading.

Thumb					
DOF	CMC_f	CMC_a	MCP_a	MCP_f	IP
M_{Fext_j} (N cm)	111	4.91	4.99	72	32
Index finger					
DOF	MCP_f		MCP_a	PIP	DIP
M_{Fext_j} (N cm)	51		−3.9	38	10

3. Optimization problem formulation

The three basic elements for the optimization problem formulation, i.e., the set of design variables, the objective function(s), and the constraints including the variables' bounding values, have to be defined for the considered study.

3.1. Design variables

In the optimization problem, the design vector $\boldsymbol{X}$ (as called in the genetic algorithm procedure) contains the independent variables of the biomechanical model. These variables include the muscle tensions vectors as specified below $\boldsymbol{F}_f$ and $\boldsymbol{F}_t$ for the index finger and for the thumb respectively, in addition to the vector $\boldsymbol{\alpha} = (\alpha_k)_{k=EDC,UI,LUM}$ which is introduced by Eq. (2) for the index finger case.

The design vector $\boldsymbol{X} = [\boldsymbol{X}_f \ \boldsymbol{X}_t]^T$ is composed of:

- $\boldsymbol{X}_f = [\boldsymbol{F}_f \ \boldsymbol{\alpha}]^T$ which contains the index finger unknowns: $\boldsymbol{F}_f = [F_{FDP} \ F_{FDS} \ F_{EDC} \ F_{EI} \ F_{LUM} \ F_{RI} \ F_{UI}]$ and $\boldsymbol{\alpha} = [a_{EDC} \ a_{LUM} \ a_{UI}]$.
- $\boldsymbol{X}_t = [F_{FPL} \ F_{EPL} \ F_{APB} \ F_{ADD} \ F_{EPB} \ F_{FPB} \ F_{APL} \ F_{OP}]^T$ which corresponds to the thumb unknown forces.

3.2. Objective functions

Objective functions based on a performance criterion of the involved muscular tensions are set to be minimized subjected to the constraints on the muscle tensions. The first objective function to be minimized is the muscle stress quadratic sum (8) [4,20]. Bolhuis et al. [21] have shown that minimization of this function favours muscle force distribution where each muscle has some contribution rather than one muscle taking the entire load.

The second objective function is the sum of all forces in the muscles (9). Minimizing the muscle forces sum leads generally to predict a muscle force distribution where the number of the activated muscles is minimum. This function (5) has been also criticized for being unable of predicting co-activation of synergistic muscles [21].

The third objective function is the maximum stress among the muscles (10) [22,23]. Minimizing this function is physiologically identical to minimizing the total fatigue of the system [21,24]. This function allocates the load to the muscles when minimizing the tension of the muscle having the highest value of stress.

$$f_1 = \sum_{i=1}^{n} \left(\frac{F_i}{PCSA_i} \right)^2 \tag{8}$$

$$f_2 = \sum_{i=1}^{n} F_i \tag{9}$$

$$f_3 = \max\left(\frac{F_i}{PCSA_i} \right) \tag{10}$$

The basic idea is to compute all possible solutions of various models when considering one, two or three objective functions out of the set given by $\{f_1, f_2, f_3\}$. Different algorithms, in which we minimize one or simultaneously multiple functions, are used to study the impact of every process on the solutions.

3.3. Constraints

The use of appropriate constraints and physiologically realistic boundary conditions can improve the solution and leads to functionally acceptable muscle tensions. These constraints are either inequalities concerning the variable bounds and the distribution coefficient or equalities dealing with the joint torques.

1) The first considered set of constraint represents the limit values of the design variables. Inequality (11) ensures positive muscle tensions, which have to be lower than the theoretical maximal isometric muscle tensions.

$$0 \leqslant F_i \leqslant F_{\max_i}, \quad i = 1, \ldots, 15 \tag{11}$$

where $F_{\max_i}$ defines the maximal isometric tension of the ith muscle in the finger computed from the following equation, $F_{\max_i} = \sigma PCSA_i$. We consider the PCSA values as given by Valero-Cuevas et al. [8] and Bouffier et al. [29] for the thumb and the index finger, respectively. The stress $\sigma = 35$ N/cm^2 is a constant value reported by Valero-Cuevas et al. [25] for all the musculoskeletal systems of the human upper limb.

2) Inequality system (12), as described by Vigouroux [11], states that the factors α_k transmitted by the muscles to the extensor mechanism bands range from 0 to 1 for the LUM and the UI muscles, and from 0 to 0.5 for the EDC muscle.

$$\begin{aligned} &0 \leqslant \alpha_{UI} \leqslant 1 \\ &0 \leqslant \alpha_{LUM} \leqslant 1 \\ &0 \leqslant \alpha_{EDC} \leqslant 0.5 \end{aligned} \tag{12}$$

3) For each degree of freedom, the following relation given the resulting torque C_{eq_j} around the joint axis can be established

$$C_{eq_j} = \tau_j - M_{Fext_j} \tag{13}$$

where:

- j is the degree of freedom at a joint that defines the flexion–extension or the abduction–adduction movement ($j = CMC_f$, CMC_a, MCP_a, MCP_f, and IP if $n =$ the thumb and $j = MCP_f$, MCP_a, PIP and DIP if $n =$ the index finger).
- M_{Fext_j} defines the torque over the jth degree of freedom (Table 3).
- τ_j defines the torque over the jth degree of freedom generated by muscles crossing the corresponding joint. The computation of each torque is established using the moment arms. The details are given in Appendix B.
- In the case of equilibrium, τ_j must balance M_{Fext_j}, which implies in this case $C_{eq_j} = 0$.

3.4. The genetic algorithm implementation

Genetic algorithms have been shown to solve linear and nonlinear problems by exploring all regions of state space and exponentially exploiting promising areas through selection, crossover and mutation applied to individuals in a population. The flowchart of the genetic algorithm is illustrated in Fig. 4 for a multi-objective optimization. We define $\boldsymbol{X}_0$ the initial population to be evaluated. $\boldsymbol{X}_0$ is created by the uniformly distributed pseudorandom numbers, using the function "rand" in Matlab and taking into account the bounds of each design variable. $\boldsymbol{X}_{est}$, $\boldsymbol{X}_{par}$ and $\boldsymbol{X}_i$ are respectively the static, the Paretian (non-dominated) and the dynamic populations for the ith iteration (Fig. 4).

For a single objective function optimization, the dashed line and dashed boxes in the block diagram are omitted (Fig. 4). For the multi-objective optimization, when optimizing all the objective functions simultaneously, the optimum solutions define the Pareto front. The algorithm scans the whole search domain and compares all the individuals to keep only those that are not dominated. Therefore, the Pareto front corresponds to the set of the non-dominated muscle tensions. For three objective functions, the Pareto front is a surface in a three-dimensional space. For a detailed description, see [26–28].

4. Results and discussions

4.1. Single objective genetic algorithm (SGA-models)

In this part we compare the results obtained by different single-objective genetic algorithm (SGA-models) based on one general function (14), in which multiple objectives f_1, f_2, and f_3 are transformed into one aggregated scalar objective function L. Each objective function is multiplied by a weighting factor (c_1, c_2, or c_3) and then a sum of all contributors is carried out. The obtained function can either represent a single optimization problem (only one c_i is non-zero) or a multi-objective problem when at least two coefficients in Eq. (14) are non-zero.

The input functions (f_1, f_2, f_3) are weighted differently to give several priorities to the objectives. In order to study the effects of the individual weighting factor on the total objective function given by Eq. (14), five SGA-models with different values of the weighting factors (c_1, c_2, and c_3) (Table 4) are carried out.

$$L(f_1, f_2, f_3) = c_1 f_1 + c_2 f_2 + c_3 f_3 \tag{14}$$

We add the squared sum $H = \sum_{j=1}^{9} (C_{eq_j})^2$ where C_{eq_j} is a relation obtained from Eq. (13). H defines the total constraint violation. It is multiplied with a penalty parameter r and the product is added to the multi-objective function value as penalty. Hence, we define the function G given by Eq. (15) which takes into account the constraint violations. For a feasible solution, the corresponding H term is zero and G becomes equal to the original function L. For an infeasible solution the G value exceeds the L computed value.

$$G(f_1, f_2, f_3) = L(f_1, f_2, f_3) + rH \tag{15}$$

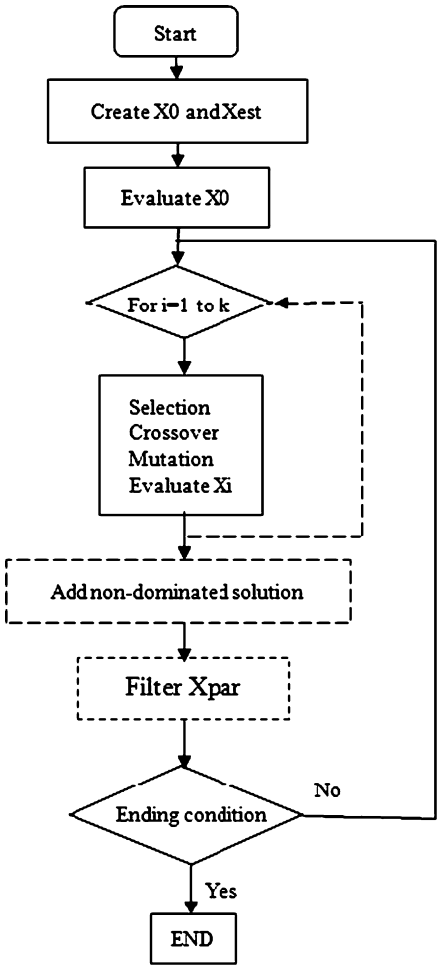

Fig. 4. The block diagram of the genetic algorithm used in both single and multi-objective optimizations. For a single objective function optimization, the dashed line and dashed boxes, in the block diagram, are omitted. $\boldsymbol{X}_0, \boldsymbol{X}_{est}$, $\boldsymbol{X}_{par}$ and $\boldsymbol{X}_i$ are respectively the initial, static, Paretian and the dynamic populations for the ith iteration.

Table 4
Weights used in the SGAs.

Weights	SGA_1	SGA_2	SGA_3	SGA_4	SGA_5
c_1	1	0	0	1/3	1/2
c_2	0	1	0	1/3	1/4
c_3	0	0	1	1/3	1/4

with $r = 100$ is the penalty parameter. Eqs. (11) and (12), which define the lower and upper bounds, are used when creating the initial population $\boldsymbol{X}_0$ at each iteration (Fig. 4).

The five objective functions are tested using the following genetic algorithm parameters:

- $N = 500$ (population size),
- Number of generation $= 300$,
- $P_c = 0.85$ (crossover probability),
- $P_m = 0.001$ (mutation probability).

All programming algorithms in Matlab are run on a minicomputer (Intel (R) core (TM) 2 DUO, Hewlett–Packard). Taking into account the implementation values stated before, the average computation time required to perform one SGA-model is equal 10 minutes.

The objective function values obtained by the application of the SGA-models are shown in Table 5. We summarize in Table 6 the results found with different SGAs for the thumb and the index muscle tensions in units of the applied forces.

Table 5
Objective function values obtained by the SGAs.

Objective function	SGA_1	SGA_2	SGA_3	SGA_4	SGA_5
f_1	141.87	209.46	321.92	178.53	166.60
f_2	64.02	57.69	100.16	69.12	69.63
f_3	8.45	10.65	7.68	8.59	8.32

Table 6
Muscle tensions (in units of applied forces) predicted by the SGAs.

Thumb muscle	SGA_1	SGA_2	SGA_3	SGA_4	SGA_5	Giurintano et al. [2]
FPL	3.52	3.40	3.19	3.58	3.46	2.44
EPL	0	0	0	0	0	0
APB	0.55	0.41	0.55	0.53	0.63	0
ADD	0.93	0.87	1.44	0.81	1.08	1.45
EPB	0	0	0	0	0	0.51
FPB	0.61	1.41	1.01	0.81	0.74	0
APL	0.41	0	3	0.39	0.84	2.54
OP	0.60	0.11	1.35	0.82	0.65	0.14
Index finger muscle	SGA_1	SGA_2	SGA_3	SGA_4	SGA_5	An et al. [7]
FDP	2.91	3.14	3.64	3.10	3.03	1.93–2.08
FDS	1.59	1.15	1.88	1.60	1.56	1.75–2.16
EDC	0.08	0	1	0	0	–
EI	0.32	0.02	1.72	0.77	0.56	–
LUM	0	0	0	0	0	0–0.72
RI	1.28	1.03	1.86	1.43	1.37	0–0.99
UI	0	0	0	0	0	0.21–0.65

The weighted sum method based on the correct selection of the weights is highly sensitive since any small perturbation in the selected weights can lead to different solutions (Table 6). In the SGA-model, the optimization process provides only one optimal solution. Since averaged values for the anatomical parameters are used, uncertainties occur in the parameter values. Hence, no SGA based optimization results are identical to those reported in the literature. This non-conformity can also be attributed to the difference between the biomechanical models used for the human fingers in each work. The obtained ratios, except for the UI muscle (see Table 6), are higher than those predicted by Giurintano et al. [2] and An et al. [7] for the thumb and the index finger, respectively. In fact, the APB, the OP and the FPB tendons show considerable activities; the FPL and the APL muscles are strongly activated also. The ADD muscle is also activated to balance the effect of the thumb abductors. The index finger extrinsic muscles, FDP, FDS, EDC, EI and RI provide the major contribution in the pinching force.

With SGA_1 and SGA_3 models, more muscles, for instance the EDC muscle, are shown to be activated. The SGA_4 and SGA_5 models do not improve the simulation results in terms of the number of activated muscles and the predicted ratios. The SGA_1 and SGA_3 models give an activation behaviour that is comparable to the one reported by Valero-Cuevas et al. [8] with the recorded EMG signals. For the two last models, a significantly activation of extrinsic extensors, particularly with SGA_3-model, is also noticed as reported by Valero-Cuevas et al. [8]. The SGA_1-model predictions are also found to be close to An et al. results. Thus, at this level, we can state that the SGA_1-model, which minimize only the muscle stress quadratic sum, and the SGA_3-model, which minimize only the maximum stress among muscles, are the best criteria compared to the three other models yielding to a real physiological interpretation.

4.2. Genetic algorithm applied in multi-objective optimization (MOGA-model)

As seen in the previous subsection, the SGA-models are not efficient in finding an acceptable tendon tensions combination. Alternatively, a genetic algorithm based on the Pareto dominance principle can be efficiently used to eliminate the above mentioned difficulties.

4.2.1. Two criteria minimization

Bi-objective optimization using genetic algorithm is implemented. We minimize two criteria simultaneously. The penalty method is also used in this case through Eq. (16). The original objective functions (f_1, f_2, f_3) are penalized proportionally to the violation of the equality constraints stated in Eq. (13). Hence, when minimizing (f_1, f_2), for instance, the two penalized functions $g(f_1)$ and $g(f_2)$, as given by Eq. (16), are minimized in the optimisation process.

The penalized functions (16) are developed in such a way that, if all constraints are satisfied, they have the values of the objectives to be minimized themselves. Otherwise, they are penalized proportionally to the discrepancy on the constraints.

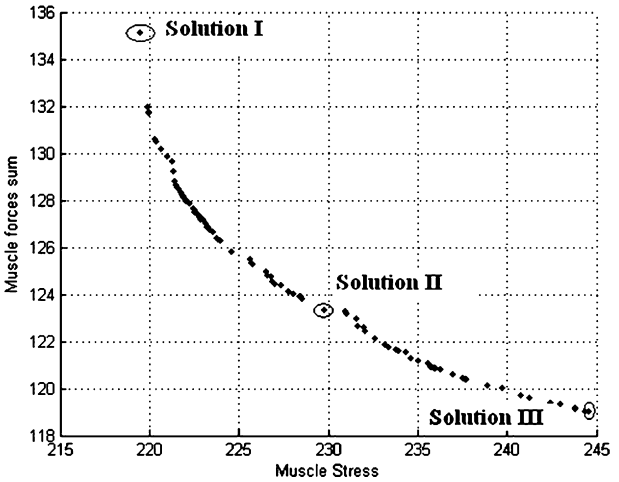

Fig. 5. The Pareto optimal curve: Set of non-dominated individuals found by genetic algorithm applied in multi-objective optimization (MOGA) when minimizing simultaneously the two penalized functions $g(f_1)$, $g(f_2)$ associated respectively to the muscle stress quadratic objective function f_1 and the muscle tensions sum function f_2. Solutions I, II and III are three different optimal design vectors.

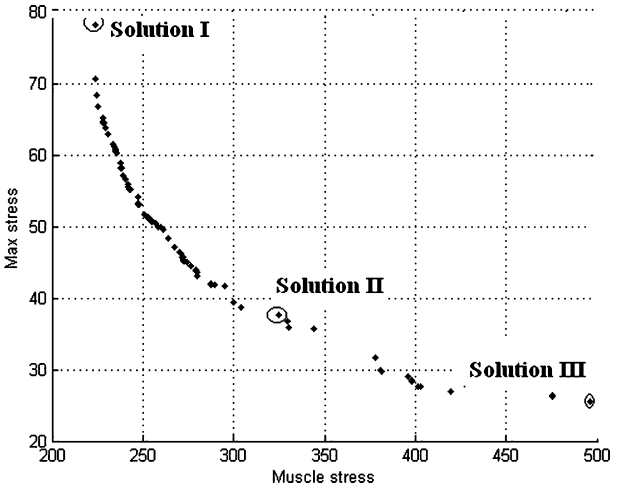

Fig. 6. The Pareto optimal curve: Set of non-dominated individuals found by genetic algorithm applied in multi-objective optimization (MOGA) when minimizing simultaneously the two penalized functions $g(f_1)$, $g(f_3)$ associated respectively to the muscle stress quadratic objective function f_1 and to the maximum of muscle stress function f_3. Solutions I, II and III are three different optimal design vectors.

The ith penalized function $g(f_i)$ is, then, given by:

$$g(f_i)_{i=1\,\text{or}\,2} = \begin{cases} f_i & \text{if } H = \sum_{j=1}^{9} (C_{eq_j})^2 = 0 \\ f_i + r \sum_{j=1}^{9} (C_{eq_j})^2 & \text{if } H = \sum_{j=1}^{9} (C_{eq_j})^2 \neq 0 \end{cases} \tag{16}$$

where $r = 100$.

For the implementation of the genetic algorithm the following parameters are used:

- $N = 500$ (population size),
- Number of generation $= 300$,
- $P_c = 0.85$ (crossover probability),
- $P_m = 0.001$ (mutation probability),
- $\delta = 0.1$ (sharing parameter).

Taking into account the implementation values stated before, the average computation time required to perform the MOGA-model when minimizing two criteria is equal to 8 minutes on the above-mentioned machine.

Figs. 5 and 6 show respectively typical plots representing the evaluations of individuals (f_1, f_2) and (f_1, f_3) inside the non-dominated filter in the objective functions. First, one can notice that the MOGA-model is able to find a diverse set of

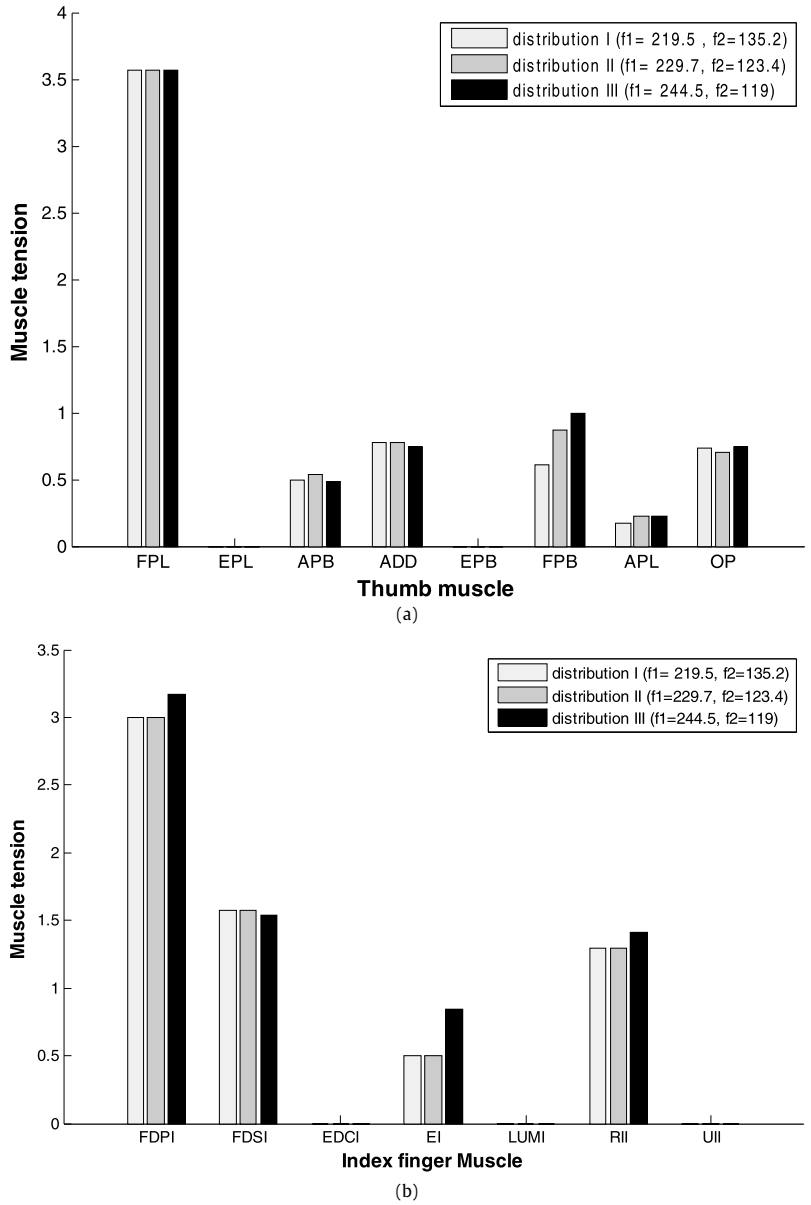

Fig. 7. (a) Thumb case. (b) Index finger case. Muscle tension distributions (in units of applied palmar fingertip force) representing respectively solutions I, II and III extracted from Pareto optimal curve corresponding to the minimization of the muscle stress quadratic sum function f_1 and the muscle tensions sum function f_2 using MOGA method.

non-dominated individuals, which yield the Pareto front. We select from the "Pareto front" (Fig. 5) three solutions: I, II and III. The corresponding design variables, the muscle tensions, are depicted in Figs. 7(a) and 7(b) for the thumb and the index finger, respectively. The simulated objective functions values for the couple (f_1, f_2) associated to solutions I, II and III are (219.5, 135.2), (229.7, 123.4), and (244.5, 119), respectively. In the case of minimizing (f_1, f_3) (Fig. 6), three solutions are also chosen and the corresponding design variables are depicted in Figs. 8(a) and 8(b) for the thumb and the index finger, respectively. The simulated objective functions values for the couple (f_1, f_3) that correspond to solutions I, II and III are respectively (223.6, 78.2), (324.6, 37.7), and (496.4, 25.5).

The normalized muscle tensions (Figs. 7(a) and 7(b)) show that, when minimizing (f_1, f_2) simultaneously, practically the same muscle activation behaviour in the three resulted distributions is obtained. The model converges towards a unique activation behaviour. However, it is not the case when minimizing (f_1, f_3) (Figs. 8(a) and 8(b)), we get significantly different distributions for the thumb and the index finger.

The EPL, EPB, LUM, and UI muscles, for the three selected solutions (Figs. 7 and 8), remain inactive when minimizing (f_1, f_2) or (f_1, f_3), respectively. These simulated results are in general identical to the ones found with the SGA-models.

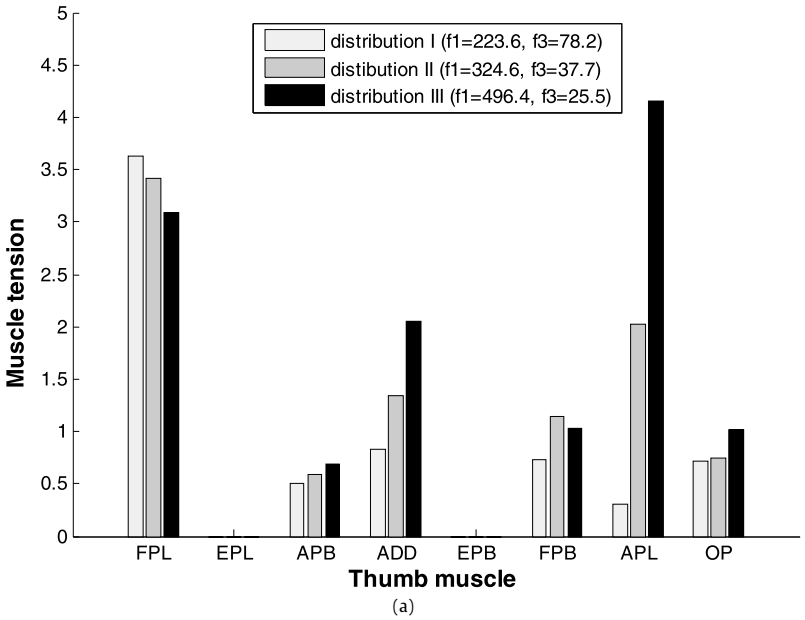

(a)

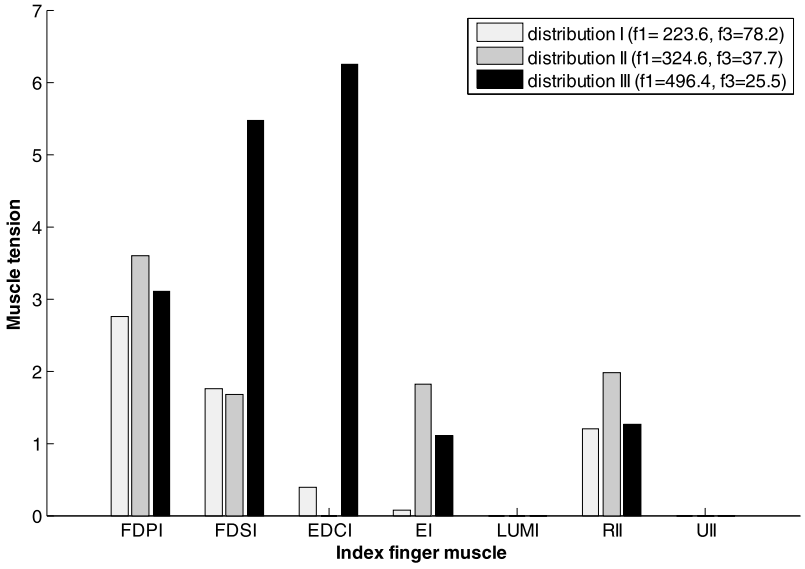

(b)

Fig. 8. (a) Thumb case. (b) Index finger case. Muscle tension distributions (in units of applied palmar fingertip force) representing respectively solutions I, II and III extracted from Pareto optimal curve corresponding to the minimization of the muscle stress quadratic sum function f_1 and the maximum of muscle stress function f_3 using MOGA method.

Minimizing (f_1, f_2) does not improve the simulated results, since the EDC is not active for all the distributions represented in Fig. 7(b). Conversely, when minimizing (f_1, f_3) the computed results (Fig. 7(b)) are close to the one measured by Valero-Cuevas et al. [8], particularly in distribution III which is the best computed solution in terms of maximum stress.

4.2.2. Three criteria minimization

Multi-objective optimization using genetic algorithm is implemented. We minimize the three criteria (f_1, f_2 and f_3) simultaneously. The use of the penalty method leads to three penalized objective functions as described in the following equation:

$$g(f_i)_{i=1,2,3} = \begin{cases} f_i & \text{if } H = \sum_{j=1}^{9} (C_{eq_j})^2 = 0 \\ f_i + r \sum_{j=1}^{9} (C_{eq_j})^2 & \text{if } H = \sum_{j=1}^{9} (C_{eq_j})^2 \neq 0 \end{cases} \tag{17}$$

The value of r is chosen to 100 as an arbitrarily large value of the penalty parameter.

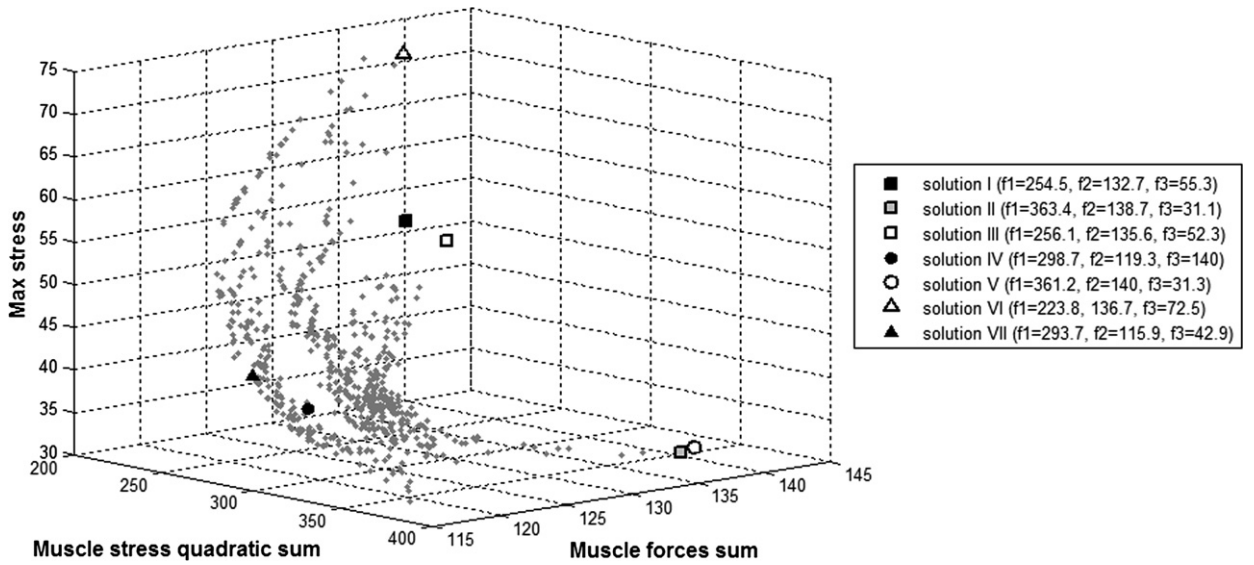

Fig. 9. Pareto front in the objective space using MOGA evolutionary process when minimizing simultaneously the three penalized functions $g(f_1)$, $g(f_2)$ and $g(f_3)$ associated respectively to the muscle stress quadratic objective function f_1, muscle tensions sum function f_2 and to the maximum of muscle stress function f_3 (initial population = 500, number of generations = 300, number of simulated non-dominated solutions = 296). Solutions I to VII are seven different optimal design vectors.

We used the same implementation parameters of the genetic algorithm as for the minimization of two criteria. The average computation time, on the same machine, required to perform a MOGA-model when minimizing the three criteria simultaneously is equal to 11 minutes.

Each point plotted in Fig. 9 belongs to the Pareto front and represents a non-dominated solution. Each non-dominated solution is defined by the three objective functions values and it corresponds to an optimal muscles tension combination. Solutions I to VII, as shown in Fig. 10, are scattered on the Pareto curve. To illustrate the diversity of the seven proposed solutions (Figs. 9 and 10), the associated distributions are given in Table 7. These optimal distributions represent a different compromise between the three criteria. Solution V, for instance, is the best if considering only the maximum muscle stress criterion. Solution VI is the best in terms of muscle stress sum optimization criterion, and solution VII is the best if considering the muscle tension sum criterion.

For all the selected solutions, we can conclude that the FPL flexor develops the highest force among all thumb muscles (Table 7). The APL muscle gets a normalized force which is higher than the SGA-models simulated ones (Table 6) but close to the one reported by Giurintano et al. [2]. The simulated APB muscle ratio does not match the one reported by Giurintano et al. work [2]. This ratio goes from 0.77 to 0.9, which is also higher than 0.4 to 0.63 (Table 6), the range of the APB ratio obtained from SGA-model simulations. The obtained value of the OP ratio is 0.6 (Table 7). It is higher than the one reported by Giurintano et al. work [2] but it remains comparable to the ratios given by the SGA-models, except for the SGA_3 one (Table 6).

In the index finger, as with the previous computed models, the UI muscle is inactive for the seven selected solutions, (Table 7). The FDP, FDS, EDC, EI and LUM muscle have ratios (see Table 7) that exceed the ones reported by An et al. [7]. The extrinsic flexors carried high muscle tensions compared to the rest of the muscles. In particular, the average value of the FDS ratio, which is equal to 2.36 (Table 6), is higher than the one reported by An et al. [7] but it is similar to the one measured experimentally in Dennerlein et al. [30].

With the MOGA-model, various tension combinations can be obtained. Up to fourteen muscles are activated at least for the selected solutions (Table 7). Solutions II and V, for example, are neighbours on the Pareto curve, get different activated muscles number, twelve and fourteen respectively. Comparing solution VI and SGA_1-model predictions leads to a similar number of activated muscles. In fact, as mentioned before, solution VI is the best in terms of muscle stress sum optimization criterion. However, we notice that the FDP muscle gets higher ratio than with the SGA_1-model. The EDC muscle is also noticed to be more activated. The EDC ratio is equal to 0.86 (Table 7) against 0.08 obtained with the SGA_1-model (Table 6).

Both solution V and the predictions of the SGA_3-model favour the minimization of the maximum muscle stress among muscle. However, solution V gets more activated muscles than SGA_3-model predictions. Furthermore, solution V has the highest ratios of the EDC and EI muscles, result which is already found with SGA_3-model and has already been proved qualitatively by the EMGs recorded by Valero-Cuevas et al. [8].

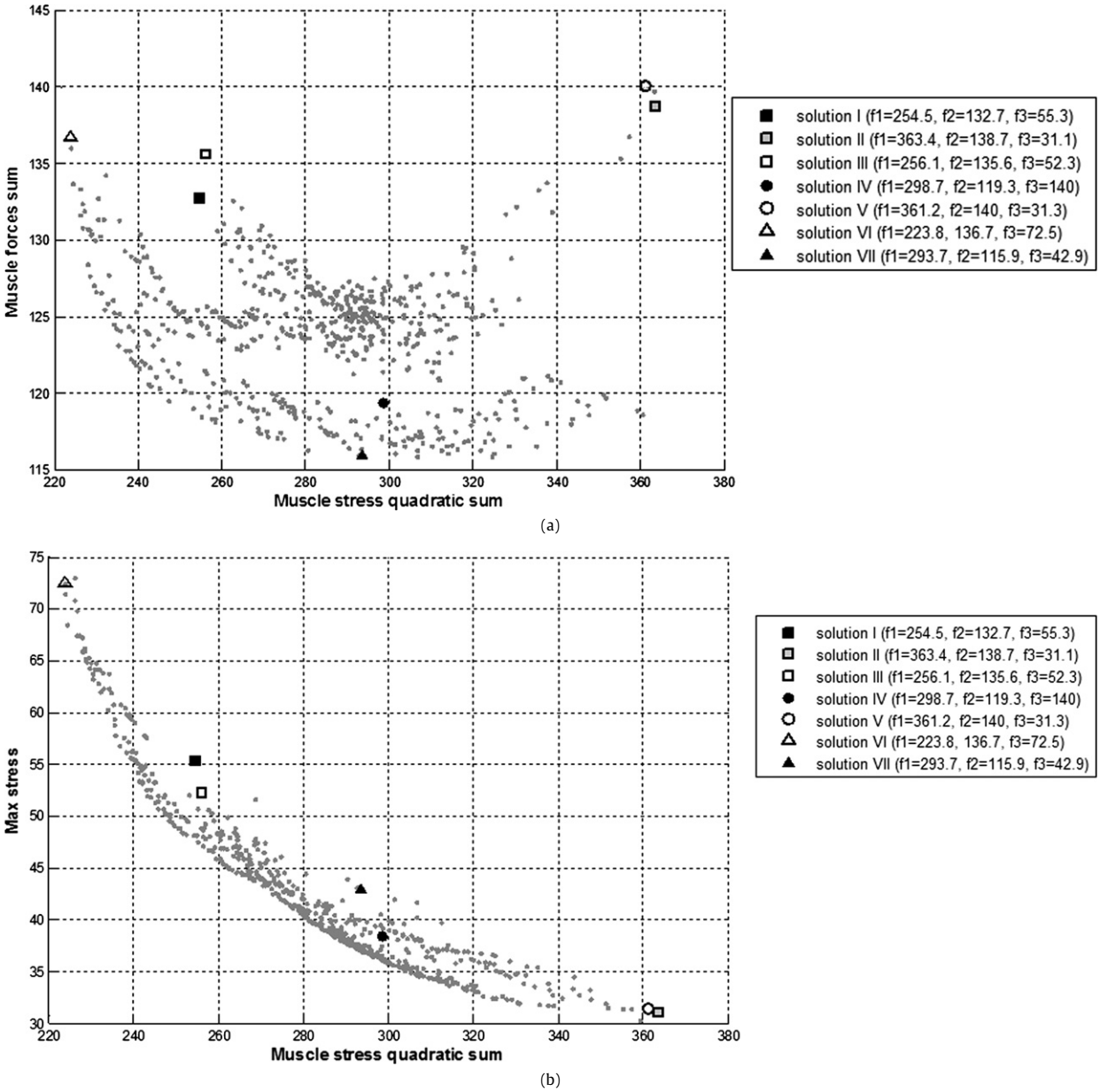

Fig. 10. (a) The f_1–f_2 objective plane. (b) The f_1–f_3 objective plane. Projection of the obtained Pareto front when minimizing simultaneously the three penalized functions $g(f_1)$, $g(f_2)$ and $g(f_3)$. Solutions I to VII are seven different optimal design vectors.

5. Conclusion

In this paper a biomechanical model of the thumb and the index finger during a tip pinch task is investigated. This study presents a theoretical analysis of various models that compares the muscular tension predictions. The problem of determining muscle tensions, as a muscular redundant one, is solved using a constrained single and multi-objective optimization base on genetic algorithms. With the MOGA-model, more antagonist muscles, such as the EPB muscle for the thumb and the EDC muscle for the index finger, are shown to be activated. Conversely, this co-contraction is not observed with the most of SGA-models even when using a weighted sum method.

Although MOGA-model process gives better tendon forces distributions than SGA-models, one needs to know, when looking for a unique pattern, which criterion among the three discussed yields the best tendon force distribution compared to MOGA-model results and to experimental data.

It has been shown, based on the performed analysis, that the principle of minimal total muscle force (SGA_2-model) predicts far fewer active muscles than indicated by EMG provides the most distant results from the experimental ones,

Table 7
Pareto optimum solutions (muscle tensions in units of applied pinch force).

Thumb muscle	Solution I	Solution II	Solution III	Solution IV	Solution V	Solution VI	Solution VII
FPL	3.27	3.26	3.27	3.27	3.31	3.46	3.36
EPL	0	0	0	0	0.05	0	0
APB	0.78	0.90	0.78	0.77	0.86	0.63	0.55
ADD	1.55	1.60	1.55	1.56	1.61	0.94	1.02
EPB	0	0.01	0	0	0.01	0	0
FPB	0.75	1.01	0.71	0.98	0.97	0.71	1.08
APL	2.19	2.32	2.01	2.27	2.33	0.35	1.03
OP	0.65	0.64	0.65	0.64	0.65	0.52	0.85
Index finger muscle	Solution I	Solution II	Solution III	Solution IV	Solution V	Solution VI	Solution VII
FDP	2.90	4.13	3.30	3.07	4.24	3.27	3.27
FDS	2.02	2.76	2.27	2.06	2.69	1.81	1.81
EDC	0.58	2.94	1.38	0.00	3.03	0.86	0
EI	0.68	1.76	0.83	1.50	1.78	0.39	0.72
LUM	0	0	0	0	0.02	0	0
RI	1.67	1.75	1.48	1.64	1.78	1.53	1.53
UI	0	0	0	0	0	0	0

in particular no co-activation of the antagonist muscles is observed. It is also interesting to notice that SGA_1 and SGA_3 models have the same weighting if considering only the number of activated muscles. However, the SGA_3-model, which minimizes the maximum stress among muscles, is the best criterion since it provides the most physiological acceptable results comparing to previous experimental results. In summary, the results of this study do not reveal only one model that gives significantly better predictions that any other model. However, it may be more advantageous and physiological to use the maximum muscle stress model, when looking for a unique pattern such as the case in motor control research.

Appendix A

A.1. Thumb Jacobian transpose matrix

θ_{1t} = CMC extension, θ_{2t} = CMC adduction, θ_{3t} = MCP adduction, θ_{4t} = MCP extension, and θ_{5t} = IP extension (Fig. 1(a)). p_{x_t}, p_{y_t} and p_{z_t} define the distances from the IP joint to contact point with object maintained.

J^T_{Thumb} is the transpose of the Jacobian matrix written in the thumb-tip coordinate frame (X_6, Y_6, Z_6).

$$J^T_{Thumb} = \begin{bmatrix} -p_{y_t} & p_{x_t} & 0 & 0 & 0 & 1 \\ -p_{y_t} + L_{MP_f}\sin\theta_{5t} & p_{x_t} + L_{MP_f}\cos\theta_{5t} & 0 & 0 & 0 & 1 \\ p_{z_t}\cos(\theta_{4t}+\theta_{5t}) & -p_{z_t}\sin(\theta_4+\theta_5) & A_{33} & \sin(\theta_{4t}+\theta_{5t}) & \cos(\theta_{4t}+\theta_{5t}) & 0 \\ \cos(\theta_{4t}+\theta_{5t})[p_{z_t}+L_{TM}\sin\theta_{3t}] & -\sin(\theta_{4t}+\theta_{5t})[p_{z_t}+L_{TM}\sin\theta_{3t}] & A_{43} & \sin(\theta_{4t}+\theta_{5t}) & \cos(\theta_{4t}+\theta_{5t}) & 0 \\ A_{51} & A_{52} & A_{53} & A_{54} & A_{55} & A_{56} \end{bmatrix}$$

$$A_{33} = -l_{MP_t}\cos\theta_{4t} + p_{y_t}\sin(\theta_{4t}+\theta_{5t}) - p_{x_t}\cos(\theta_{4t}+\theta_{5t})$$
$$A_{43} = p_{y_t}\sin(\theta_{4t}+\theta_{5t}) - l_{MP_t}\cos\theta_{4t} - l_{TM}\cos\theta_{3t} - p_{x_t}\cos(\theta_{4t}+\theta_{5t})$$
$$A_{51} = p_{z_t}\sin(\theta_{4t}+\theta_{5t})\sin(\theta_{2t}+\theta_{3t}) - p_{y_t}\cos(\theta_{2t}+\theta_{3t}) + l_{MP_t}\sin(\theta_{5t}) + \cos(\theta_{2t}+\theta_{3t}) + l_{TM}\sin(\theta_{4t}+\theta_{5t})\cos\theta_{2t}$$
$$A_{52} = p_{x_t}\cos(\theta_{2t}+\theta_{3t}) + p_{z_t}\cos(\theta_{4t}+\theta_{5t})\sin(\theta_{2t}+\theta_{3t}) + l_{MP_t}\cos\theta_{5t}\cos(\theta_{2t}+\theta_{3t}) + l_{TM}\cos(\theta_{4t}+\theta_{5t})\cos\theta_{2t}$$
$$A_{53} = -p_{x_t}\sin(\theta_{4t}+\theta_{5t})\sin(\theta_{2t}+\theta_{3t}) - p_{y_t}\cos(\theta_{4t}+\theta_{5t})\sin(\theta_{2t}+\theta_{3t}) - l_{MP_t}\sin(\theta_{2t}+\theta_{3t})\sin(\theta_{4t})$$
$$A_{54} = -\cos(\theta_{4t}+\theta_{5t})\sin(\theta_{2t}+\theta_{3t})$$
$$A_{55} = \sin(\theta_{4t}+\theta_{5t})\sin(\theta_{2t}+\theta_{3t})$$
$$A_{56} = \cos(\theta_{2t}+\theta_{3t})$$

A.2. Index finger's Jacobian transpose matrix

θ_{1f} = MCP extension, θ_{2f} = MCP adduction, θ_{3f} = PIP extension, and θ_{4f} = DIP extension (Fig. 1(b)). p_{x_f}, p_{y_f}, and p_{z_f} define the distances from the DIP joint to the contact point.

J^T_{Index} is the transpose of the index finger Jacobian matrix written in the index-tip coordinate frame (X_5, Y_5, Z_5).

$$J_{Index}^{T}=\begin{bmatrix} -p_{y_f} & p_{x_f} & 0 & 0 & 0 & 1\\ -p_{y_f}+L_{MP_f}\sin\theta_{4f} & p_{x_f}+L_{MP_f}\cos\theta_{4f} & 0 & 0 & 0 & 1\\ A_{31} & A_{32} & A_{33} & \sin\theta_{2f} & -\cos\theta_{2f} & 0\\ A_{41} & A_{42} & A_{43} & -\sin\theta_{2f}\cos(\theta_{3f}+\theta_{4f}) & \sin\theta_{2f}\sin(\theta_{3f}+\theta_{4f}) & \cos\theta_{2f} \end{bmatrix}$$

$$\begin{aligned}
A_{31} &= -\cos\theta_{2f}\cos(\theta_{3f}+\theta_{4f})\big(p_{x_f}\sin\theta_{2f}\cos(\theta_{3f}+\theta_{4f})-p_{y_f}\sin\theta_{2f}\sin(\theta_{3f}+\theta_{4f})\\
&\quad+(l_{PP_f}+l_{MP_f}\cos\theta_{3f})\sin\theta_{2f}-p_{z_f}\cos\theta_{2f}\big)\\
A_{32} &= -\sin\theta_{2f}\cos(\theta_{3f}+\theta_{4f})\big(p_{x_f}\sin\theta_{2f}\cos(\theta_{3f}+\theta_{4f})-p_{y_f}\sin\theta_{2f}\sin(\theta_{3f}+\theta_{4f})\\
&\quad+l_{MP_f}\sin\theta_{2f}\cos\theta_{3f}-p_{z_f}\cos\theta_{2f}+l_{PP_f}\sin\theta_{2f}\big)\\
A_{33} &= p_{x_f}\big[\cos(\theta_{2f}+\theta_{3f}+\theta_{4f})\cos(\theta_{3f}+\theta_{4f})\big]+p_{y_f}\big[-\cos(\theta_{3f}+\theta_{4f})\sin(\theta_{2f}+\theta_{3f}+\theta_{4f})+\sin\theta_{2f}\big]\\
&\quad+p_{z_f}\sin(\theta_{2f}+\theta_{3f}+\theta_{4f})+l_{MP_f}\cos\theta_{3f}\cos(\theta_{2f}+\theta_{3f}+\theta_{4f})+l_{PP_f}\cos(\theta_{2f}+\theta_{3f}+\theta_{4f})\\
A_{41} &= p_{z_f}\sin\theta_{2f}\sin(\theta_{3f}+\theta_{4f})-\cos\theta_{2f}\big(p_{y_f}-l_{PP_f}\sin(\theta_{3f}+\theta_{4f})-l_{MP_f}\sin\theta_{4f}\big)\\
A_{42} &= \cos\theta_{2f}\big(p_{x_f}+l_{PP_f}\cos(\theta_{3f}+\theta_{4f})+l_{MP_f}\cos\theta_{4f}\big)+p_{z_f}\sin\theta_{2f}\cos(\theta_{3f}+\theta_{4f})\\
A_{43} &= \sin\theta_{2f}\big(-p_{y_f}\cos(\theta_{3f}+\theta_{4f})+l_{MP_f}\cos(\theta_{3f}+\theta_{4f})\sin\theta_{4f}-p_{x_f}\sin(\theta_{3f}+\theta_{4f})\\
&\quad-l_{MP_f}\sin(\theta_{3f}+\theta_{4f})\cos\theta_{4f}\big)
\end{aligned}$$

Appendix B

The moment over the jth degree of freedom is computed according to the following equation: $\tau_j=\sum_i r_{ij}F_i$. $j=CMC_f$, CMC_a, MCP_a, MCP_f, and IP for the thumb. $j=MCP_f$, MCP_a, PIP and DIP for the index finger, where:

- r_{ij} is the distance from the ith muscle's line of action to the jth joint centre of rotation defining the moment arm. r_{ij}'s values are reported by Smutz et al. [31] for the muscles of the thumb and by Valero-Cuevas et al. [8] for the muscle of the index finger.
- F_i is the tension of the ith muscle.

B.1. Joint torques for the thumb

$$\begin{aligned}
\tau_{IP} &= -F_{FPL}r_{FPL/IP}+F_{EPL}r_{EPL/IP}\\
\tau_{MCP_f} &= -F_{FPL}r_{FPL/MCP_f}-F_{APB}r_{APB/MCP_f}-F_{ADD}r_{ADD/MCP_f}-F_{FPB}r_{FPB/MCP_f}+F_{EPL}r_{EPL/MCP_f}+F_{EPB}r_{EPB/MCP_f}\\
\tau_{MCP_a} &= F_{FPL}r_{FPL/MCP_a}+F_{EPL}r_{EPL/MCP_a}+F_{ADD}r_{ADD/MCP_a}-F_{FPB}r_{FPB/MCP_a}-F_{EPB}r_{EPB/MCP_a}-F_{APB}r_{APB/MCP_a}\\
\tau_{CMC_a} &= -F_{FPL}r_{FPL/CMC_a}-F_{FPB}r_{FPB/CMC_a}-F_{EPB}r_{EPB/CMC_a}-F_{APL}r_{APL/CMC_a}-F_{APB}r_{APB/CMC_a}+F_{EPL}r_{EPL/CMC_a}\\
&\quad+F_{ADD}r_{ADD/CMC_a}+F_{OP}r_{OP/CMC_a}\\
\tau_{CMCf} &= -F_{FPL}r_{FPL/CMC_f}-F_{FPB}r_{FPB/CMC_f}-F_{APB}r_{APB/CMC_f}-F_{ADD}r_{ADD/CMC_f}-F_{OP}r_{OP/CMC_f}+F_{EPL}r_{EPL/CMC_f}\\
&\quad+F_{EPB}r_{EPB/CMC_f}+F_{APL}r_{APL/CMC_f}
\end{aligned}$$

B.2. Joint torques for the index finger

$$\begin{aligned}
\tau_{DIP} &= -F_{FDP}r_{FDP/DIP}+F_{TE}r_{TE/DIP}\\
\tau_{PIP} &= -F_{FDP}r_{FDP/PIP}-F_{FDS}r_{FDS/PIP}+F_{ES}r_{ES/PIP}+F_{RB}r_{RB/PIP}+F_{UB}r_{UB/PIP}\\
\tau_{MCP_a} &= F_{FDP}r_{FDP/MCP_a}+F_{FDS}r_{FDS/MCP_a}+F_{UI}r_{UI/MCP_a}+F_{EI}r_{EI/MCP_a}-F_{LUM}r_{LUM/MCP_a}-F_{RI}r_{RI/MCP_a}\\
&\quad-F_{EDC}r_{EDC/MCP_a}\\
\tau_{MCP_f} &= -F_{FDP}r_{FDP/MCP_f}-F_{FDS}r_{FDS/MCP_f}-F_{LUM}r_{LUM/MCP_f}-F_{UI}r_{UI/MCP_f}-F_{RI}r_{RI/MCP_f}+F_{EDC}r_{EDC/MCP_f}\\
&\quad+F_{EI}r_{EI/MCP_f}
\end{aligned}$$

References

[1] G.E. Omer, Tendon transfers for traumatic nerve injuries, Journal of Hand Surgery (Am. Volume) 4 (3) (2004) 214–226.
[2] D.J. Giurintano, A.M. Hollister, W.L. Buford, D.E. Thompson, L.M.A. Myers, Virtual five-link model of the human, Medical Engineering & Physics 4 (1995) 297–303.
[3] K.N. An, E.Y. Chao, W.P. Cooney, R.L. Linscheid, Normative model of human hand for biomechanical analysis, Journal of Biomechanics 12 (10) (1979) 775–788.

[4] R. Raikova, B.I. Prilutsky, Sensitivity of predicted muscle tensions to parameters of the optimization-based human leg model revealed by analytical and numerical analyses, Journal of Biomechanics 34 (2001) 1243–1255.
[5] M. Praagman, H.E.J. Veeger, F.C.T. Vander Helm, E.K.J. Chadwick, Relationship between mechanical objective functions and muscle oxygen consumption, Journal of Biomechanics 39 (4) (2006) 758–765.
[6] R. Ait-Haddou, A. Jinha, W. Herzog, P. Binding, Analysis of the force-sharing problem using an optimization model, Mathematical Biosciences 191 (2) (2004) 111–122.
[7] K.N. An, E.Y. Chao, W.P. Cooney, R.L. Linscheid, Forces in the normal and abnormal hand, Journal of Orthopaedic Research 3 (1985) 202–211.
[8] F.J. Valero-Cuevas, F.E. Zajac, C.G. Burgar, Large index-fingertip forces are produced by subject-independent patterns of muscle excitation, Journal of Biomechanics 31 (8) (1998) 693–703.
[9] W.P. Cooney, E.Y.S. Chao, Biomechanical analysis of static forces in the thumb during hand function, Journal of Bone and Joint Surgery 59A (1977) 27–36.
[10] N. Brook, J. Mizrahi, M. Shoham, J. Dayan, A biomechanical model of index finger dynamics, Medical Engineering and Physics 17 (1) (1995) 54–63.
[11] L. Vigouroux, Estimation of finger muscle tendon tensions and pulley forces during specific sport—climbing grip techniques, Journal of Biomechanics 39 (14) (2006) 2583–2592.
[12] O. Gundogdu, K.S. Anderson, M. Parnianpour, Development of a genetic algorithm based biomechanical simulation of sagittal lifting tasks, Biomedical Engineering Applications, Basis & Communications 17 (1) (2005) 12–18.
[13] Y. Toshev, S. Monchaud, Une approche heuristique appliquée en biomécanique (Heuristic approach to biomechanical application), Comptes rendus de l'Académie des sciences, Série II, Mécanique, physique, chimie, astronomie 325 (3) (1997) 135–142.
[14] W. Stadler, A survey of multicriteria optimization, or the vector maximum problem, Journal of Optimization Theory and Applications 29 (1979) 1–52.
[15] D.E. Goldberg, Genetic Algorithms in Search, Optimization and Machine Learning, 1st ed., Addison-Wesley, USA, 1989.
[16] C. Fonseca, P. Fleming, An overview of evolutionary algorithms in multi-objective optimization, Evolutionary Computation 3 (1995) 1–18.
[17] S.L. Ho, Y. Shiyou, H.C. Wong, N. Guangzheng, A simulated annealing algorithm for multi-objective optimizations of electromagnetic devices, IEEE Transactions on Magnetics 39 (3) (2003) 1285–1288.
[18] D.G. Kamper, H.C. Fischer, E.G. Cruz, Impact of finger posture on mapping from muscle activation to joint torque, Clinical Biomechanics 21 (2001) 361–369.
[19] A.B. Sghaier, L. Romdhane, F.B. Ouezdou, Applying robotics principles for the analysis of key fingered grip with normal and abnormal human hands, in: Proceeding of IEEE/RSJ International Conference on Robotic and Automation, USA, 2007, pp. 2963–2968.
[20] W. Maurel, 3D modeling of the human upper limb including the biomechanics of joints, muscles and soft tissues, PhD thesis, Ecole Polytechnique Federale de Lausanne, 1999.
[21] B.M. Van Bolhuis, C.C. Gielen, A comparison of models explaining muscle activation patterns for isometric contractions, Biological Cybernetics 81 (3) (1999) 249–261.
[22] K.N. An, B.M. Kwak, E.Y. Chao, B.F. Morrey, Determination of muscle and joint forces: a new technique to solve the indeterminate problem, Journal of Biomechanical Engineering 106 (1984) 364–367.
[23] J. Rasmussen, M. Damsgaard, M. Voigt, Muscle recruitment by the min/max criterion: a comparative numerical study, Journal of Biomechanics 34 (2001) 409–415.
[24] J. Dul, G.E. Johnson, R. Shiavi, M.A. Townsend, Muscular synergism. II: A minimum-fatigue criterion for load sharing between synergistic muscles, Journal of Biomechanics 17 (9) (1984) 675–684.
[25] F.J. Valero-Cuevas, M.E. Johanson, J.D. Towles, Towards a realistic biomechanical model of the thumb: the choice of kinematic description may be more critical than the solution method or the variability/uncertainty of musculoskeletal parameters, Journal of Biomechanics 36 (2003) 1019–1030.
[26] R.Q. Sardinas, M.R. Santana, E.A. Brindis, Genetic algorithm-based multi-objective optimization of cutting parameters in turning processes, The International Journal of Advanced Manufacturing Technology 16 (2006) 127–133.
[27] L. Chen, J. McPhee, W.G. Yeh, A diversified multi-objective GA for optimizing reservoir rule curves, Advances in Water Resources 30 (5) (2007) 1082–1093.
[28] M.N.A. Pereira, Evolutionary multicriteria optimization in core designs: basic investigations and case study, Annals of Nuclear Energy 31 (2004) 1251–1264.
[29] V. Bouffier, B. Leroy, Modélisation et simulation du membre supérieur droit, in: Journée thématique de la société de Biomécanique "Humanoides", Valenciennes, France, 2004.
[30] J.T. Dennerlein, E. Diao, C.D. Mote, D.M. Rempel, Tension of the flexor digitorum superficialis tendon is higher than a current model predicts, Journal of Biomechanics 31 (4) (1998) 289–305.
[31] W.P. Smutz, A. Kongsayreepong, R.E. Hughes, G. Niebur, W.P. Cooney, K.N. An, Mechanical advantage of the thumb muscles, Journal of Biomechanics 31 (1998) 565–570.